# Mid-Infrared Hyperspectral Simulator for Laser-Based Detection of Trace Chemicals on Surfaces*

Travis Myers[a], Derek Wood[a], Anish K. Goyal[†a], David Kelley[a], Petros Kotidis[a], Gil Raz[b], Cara Murphy[b], and Chelsea Georgan[b]

[a]Block Engineering/MEMS, 377 Simarano Drive, Marlborough, MA 01752
[b]Systems and Technology Research, 600 W. Cummings Park, Suite 6500, Woburn, MA 01801

## ABSTRACT

Laser-based, mid-infrared (MIR) hyperspectral imaging (HSI) has the potential to detect a wide range of trace chemicals on a variety of surfaces under standoff conditions. The major challenge of MIR reflection spectroscopy is that the reflection signatures for surface chemicals can be complex and exhibit significant spectral variability. This paper describes a MIR Hyperspectral Simulator that is being developed to model the reflectance signatures from surfaces including the effects of speckle and other sources of spectral variability. Simulated hypercubes will be compared with experiments.

**Keywords:** infrared spectroscopy, vibrational spectroscopy, hyperspectral imaging, chemical detection, standoff detection

## 1. INTRODUCTION

The mid-infrared (MIR) portion of the optical spectrum spans roughly $\lambda \approx 2.5$ to 14 μm (in wavenumbers, $\bar{\nu} = c/\lambda \approx$ 4000 to 700 $cm^{-1}$) and contains the mid-wave infrared (MWIR) and long-wave infrared (LWIR) atmospheric transmission windows along with the so-called "molecular fingerprint region." MIR spectroscopy is a standard laboratory method for identifying and characterizing chemicals. Laser-based, MIR hyperspectral imaging (HSI) is a method for detecting a wide range of trace chemicals on surfaces at standoff distances of many 10's of meters at high speed, with high sensitivity, and using a sensor that is intrinsically eye-safe. This is enabled by the fact that almost all chemicals have unique MIR absorption spectra with absorption cross-sections that can be very large [1-5].

The major challenge of MIR reflection spectroscopy is that the reflection signatures for surface chemicals can be complex and exhibit significant spectral variability. Reflection spectra often depend on parameters such as chemical concentration, particle size distribution (for solids), substrate material, substrate roughness, viewing angle, etc. Furthermore, measured reflection signatures often include speckle, which adds significant noise. In order to fully utilize the potential of MIR reflection spectroscopy for standoff chemical detection, it is imperative that reflectance models for contaminated surfaces be developed to explicitly include as many factors affecting signature variability as possible [6,7]. These models will then facilitate the further development of detection & classification algorithms [8].

This paper describes a MIR Hyperspectral Simulator (i.e., "HSI Simulator") that has been developed to model reflectance signatures of chemicals on surfaces. The goal is to develop a simulator that matches experimental results with enough fidelity to allow for the development of detection algorithms that are relevant across a wide range of real-world conditions. In addition to incorporating multiple precise, physically-motivated spectral models of contaminated surfaces, our simulator also explicitly includes effects of detector noise and speckle at each pixel of a HgCdTe (MCT) focal-plane array (FPA) when illuminated by a wavelength-tunable laser.

* This research was funded by the Office of the Director of National Intelligence (ODNI), Intelligence Advanced Research Projects Activity (IARPA), through the AFRL contract FA8650-16-C-9107. All statements of fact, opinion or conclusions contained herein are those of the authors and should not be construed as representing the official views or policies of IARPA, the ODNI, or the U.S. Government. The Government is authorized to reproduce and distribute reprints for Governmental purposes notwithstanding any copyright annotation thereon.
† Corresponding author: anish.goyal@blockeng.com

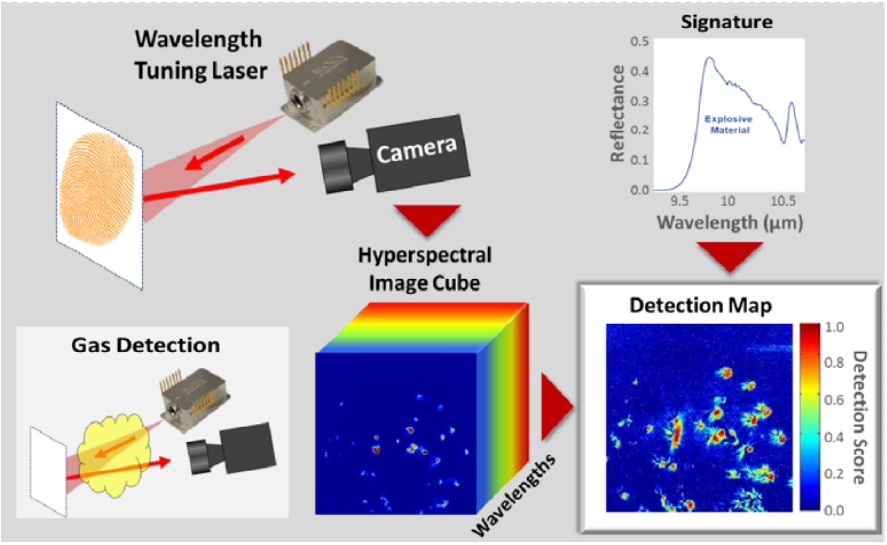


Figure 1: Concept of laser-based mid-infrared (MIR) hyperspectral imaging (HSI).

## 2. MODELS FOR LASER-BASED MIR HYPERSPECTRAL IMAGING

Figure 1 depicts the concept of MIR HSI, where a wavelength-tunable laser illuminates a surface and the reflected light is captured by a camera. As the laser wavelength is tuned, images are captured by the camera at each excitation wavelength to generate a hyperspectral image cube (i.e., "hypercube"). After appropriate normalization for laser illumination intensity and system throughput, this hypercube contains the reflectance of the target surface relative to that of a reference surface. Each frame of the hypercube contains an image of the surface reflectance at a particular wavelength, and likewise each pixel contains the full spectral reflectance at a particular point on the target. These spectra can subsequently be compared to a library of reference signatures in order to identify each chemical contaminant. As shown in Figure 1, gases that are present between the sensor and the surface can also be detected and identified based on their MIR absorption spectra.

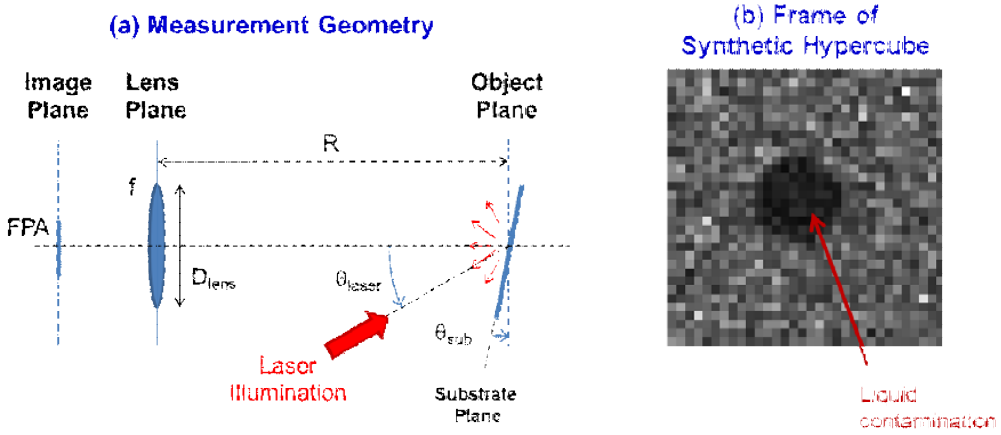


Figure 2: (a) Geometry of HSI Simulator and (b) a frame of a synthetic hypercube for a surface containing a circular region of chemical contamination.

### 2.1 Model Parameters

The geometry that is used by the HSI Simulator to calculate synthetic hypercubes is shown in Figure 2a. The angle of laser illumination and sample orientation are defined with respect to the camera axis. The primary input parameters are

- Geometry: distance from camera lens to surface of interest
- Camera: pixel size, number of pixels in hypercube, D*, quantum efficiency, integration time
- Receiver: focal length, lens diameter, optical throughput
- Laser: list of wavelengths, illumination intensity, polarization, illumination angle
- Surface: material, sample angle, roughness parameters
- Chemical: chemical identification number, loading, appropriate signature model
- Speckle: enable or disable

Figure 2b shows a frame of a synthetic hypercube frame with 32x32 pixels of a surface that has been contaminated with a liquid. This hypercube includes both detector noise and speckle noise. The sections that follow describe the basic framework used to calculate these synthetic hypercubes.

### 2.2 Received Power

The total power received by the camera, $P_{receiver}$, is calculated using [1]

$$P_{receiver} = P_{laser} \cdot \rho_{\Omega} \cdot \Omega \cdot T \qquad (3)$$

where $P_{laser}$ is the incident laser power, $\Omega$ is the solid angle of the receiver, and $T$ is a factor that represents all transmission losses. If the surface is at a distance $L$ from the camera lens and is imaged onto the FPA using a lens with effective focal length $f$ and diameter $D_{lens}$, the solid angle for the receiver is given by

$$\Omega = 2\pi\left[1 - \frac{L}{\sqrt{L^2 + \left(D_{lens}/2\right)^2}}\right] \approx \pi\left(\frac{D_{lens}}{2L}\right)^2 .$$

The scattering from a surface is characterized by the bi-directional reflectance distribution function (BRDF), which includes the spectral signature of the chemical/surface combination. The BRDF is defined as

$$\rho_{\Omega} = \frac{\text{radiance at detector}}{\text{irradiance of illumination}}$$

where the "radiance at detector" is the collected power per unit area per unit solid angle of the receiver, and the "irradiance of illumination" is the incident laser power per unit area in a plane that is normal to the illumination direction. The BRDF thus has units of inverse steradians, $sr^{-1}$. For signal-to-noise (SNR) calculations, the signal power at each pixel, $P_{pix}$, is of primary interest. Each pixel of the FPA images a region on the target having a size called the ground sampling distance (GSD) which is given by

$$GSD = \left(\frac{L}{f} - 1\right) d_{pix} \approx \frac{L}{f} d_{pix}$$

where $d_{pix}$ is the physical diameter of each pixel on the detector and $f$ is the focal length of the collecting lens. The total power received per pixel can be written in terms of the laser irradiance $I_{laser}$ (power per unit area), as

$$P_{pix} = \left( I_{laser} GSD^2 \right) \rho_\Omega \, \Omega \cdot T \quad \approx I_{laser} \cdot \rho_\Omega \cdot \frac{\pi}{4} \left( \frac{d_{pix}}{f/\#} \right)^2 \cdot T$$

where the f-number of the lens $f/\# = f/D_{lens}$. Since the BRDF has units of inverse steradians, it is convenient to convert this value to a reflectance relative to a reference substrate. We choose this reference substrate to be a perfect Lambertian scatterer, which has a constant BRDF given by $\rho_\Omega = \pi^{-1}\,\mathrm{sr}^{-1}$. The reflectance measured at each pixel of the hypercube is then calculated using

$$R_{sample} = \frac{\rho_{\Omega,sample}}{\rho_{\Omega,Lambertian}} = \rho_{\Omega,sample} \cdot (\pi\,\mathrm{sr}).$$

The preceding equations is what is calculated by the HSI Simulator. Experimentally, we have use a sandblasted aluminum as a reference substrate; it is spectrally neutral, but has a BRDF that is roughly 2-times higher than a perfect Lambertian scatterer at small angles. This additional factor is incorporated into the calculation of the reflectance spectra such that the hypercube is normalized to a perfect Lambertian-scattering surface.

### 2.3 Substrate Models

The BRDF of any substrate is defined as a function of the wavelength, incident angle, and emittance angle of the laser illumination. In most cases, the BRDF of the substrate can separated into terms that are dependent upon wavelength and angle,

$$\rho_{\Omega,sub} = R_{sub}(\lambda) \cdot N_{sub}(\theta_{offset})$$

where

| | |
|---|---|
| $R_{sub}(\lambda)$ | wavelength-dependent term of the substrate BRDF |
| $N_{sub}(\theta_{offset})$ | normalized angular-dependent term of the substrate BRDF; |
| $\theta_{offset}$ | angular offset between specular reflection direction and the receiver |

For a perfect Lambertian scatterer, $R_{sub} = 1$ and $N_{sub} = 1/\pi\ \mathrm{sr}^{-1}$. The angular portion of the BRDF can be approximated as a sum of exponential terms using

$$N_{sub}(\theta_{offset}) = \sum_n a_n \exp(-b_n \theta_{offset}) \ .$$

We have found this approximation to be accurate in describing many surfaces of interest at modest offset angles (e.g., <30°). It is usually most convenient to normalize $N_{sub}$ such that the integrated scattering intensity over all directions is unity. In this case, the wavelength dependent portion of the BRDF can be obtained from hemispherical reflectance measurements. Alternatively, it can be inferred from the complex index of the substrate, $n_{sub}$, using $R_{sub} = \left| (n_{sub} - 1)/(n_{sub} + 1) \right|^2$.

### 2.4 Data for Chemicals

The HSI Simulator incorporates spectral data for hundreds of chemicals. This includes complex refractive index data for liquids, powder reflectance data for solids, and absorbance data for vapors. As an example, Figure 3 plots the extinction coefficient (i.e., absorption coefficient) for several liquids in the database. The extinction coefficient is color coded as a

function of wavenumber (and wavelength) over the MIR band in which red represents strongly absorbing bands. Based on this plot, one can readily see why the wavelength range between about 6 – 13 μm is called the "molecular fingerprint region."

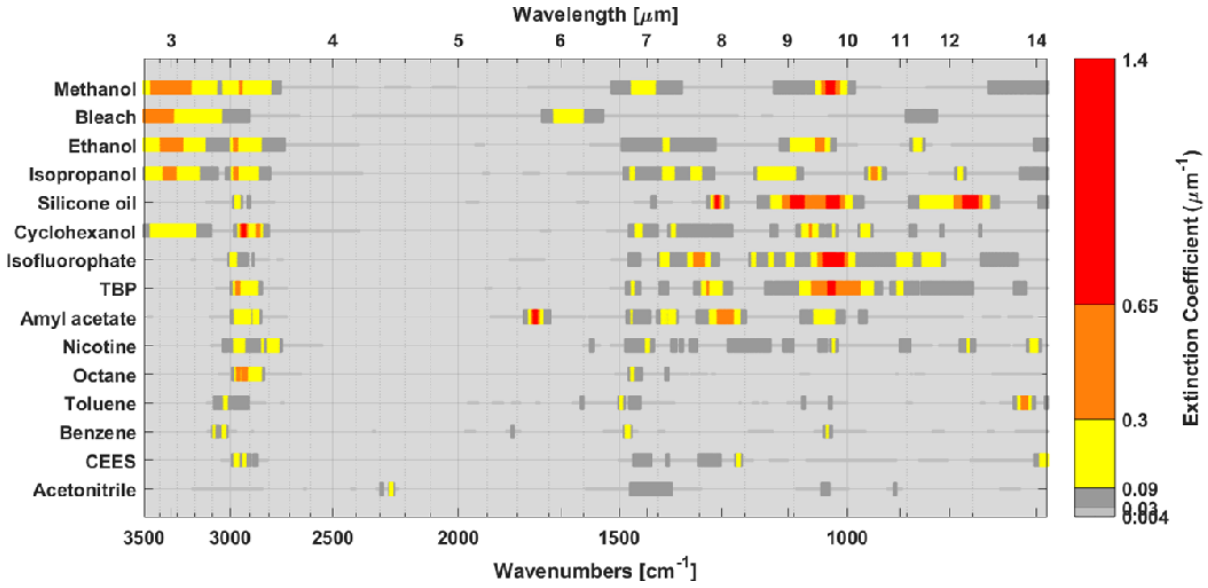


Figure 3: Color-coded presentation of the extinction coefficient for several liquids versus wavenumber (wavelength is indicated on the top axis). Note that the wavenumber scale is non-linear to facilitate plotting over a wide range.

### 2.5 Model for Liquid-Contaminated Surfaces

The physical model being used to simulate liquid-contaminated surfaces is depicted in Figure 4. The Transfer Matrix Method (TMM) is used to exactly calculate the reflectance due to a film (or multilayer film) on a substrate assuming that the interfaces are both smooth and parallel [9]. As a direct result of these two assumptions, there is (in principle) only a specular reflection from the target. But, since the HSI Simulator is primarily concerned with non-specular reflection conditions, the BRDF for the contaminated surface is approximated as the product of the reflectance calculated using the TMM and the angular portion of the substrate's BRDF under the assumption that $N_{sub}$ is normalized.

Figure 4 plots example spectra for a 1-μm-thick film of silicone oil on both metallic (perfect metal) and dielectric (polyethylene) substrates. For case of the metallic substrate, the reflectance is reduced at those wavelengths where the silicone oil is absorbing. For the case of a dielectric substrate, the reflectance is enhanced at those wavelengths where the silicone oil is absorbing, and results in an inverted spectrum compared to the metallic substrate. This effect is expected based on the physics of the interfacial boundary conditions [1,6].

We plan to continue to refine the signature models to more closely match experiments. This will include extending the TMM to take into account the fact that the surfaces are, in fact, rough rather than smooth. We also plan to incorporate additional models for cases where the contamination cannot be treated as a conformal thin film on a surface. This will involve defining the most likely applicable signature models for a particular combination of surface, chemical, and deposition conditions.

### 2.6 Noise Models

The HSI Simulator currently incorporates models for both detector noise and speckle noise. The detector noise is calculated based on the pixel's specific detectivity, or D*. Detector noise models that more closely match the performance of the actual MCT FPA being used including, for example, readout noise can also be incorporated.

In many cases, the spectral variability is dominated by speckle. It is, therefore, very important to incorporate this phenomenon in the HSI Simulator. The general approach for incorporating speckle is show in Figure 5. First, the reflected amplitude is calculated for each subpixel at the target using the relevant signature model. This reflection amplitude is then multiplied by a phase factor that is related to the local height of the surface, where the surface roughness is assumed to be Gaussian distributed. By performing a Fast-Fourier Transform (FFT) on the resulting amplitude distribution, one obtains the speckle pattern in the aperture plane of the camera lens. A subsequent FFT calculates the amplitude of the speckle pattern at the camera FPA. The amplitudes are then converted to local intensity, and results are binned on a pixel basis to yield the final hypercube. The statistics of the speckle patterns calculated using this method are consistent with theory [10].

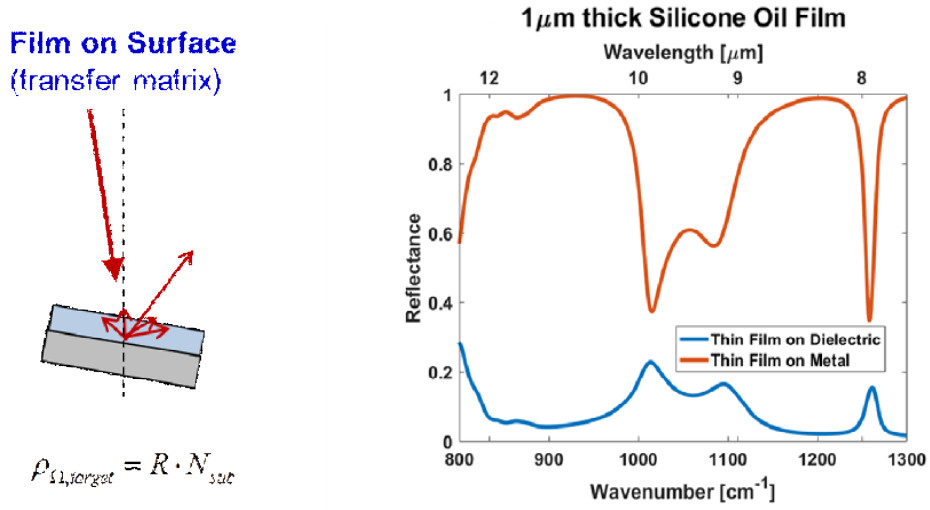


Figure 4: (left) Model for liquid chemicals and (right) calculated results for silicone oil on dielectric and metallic surfaces.

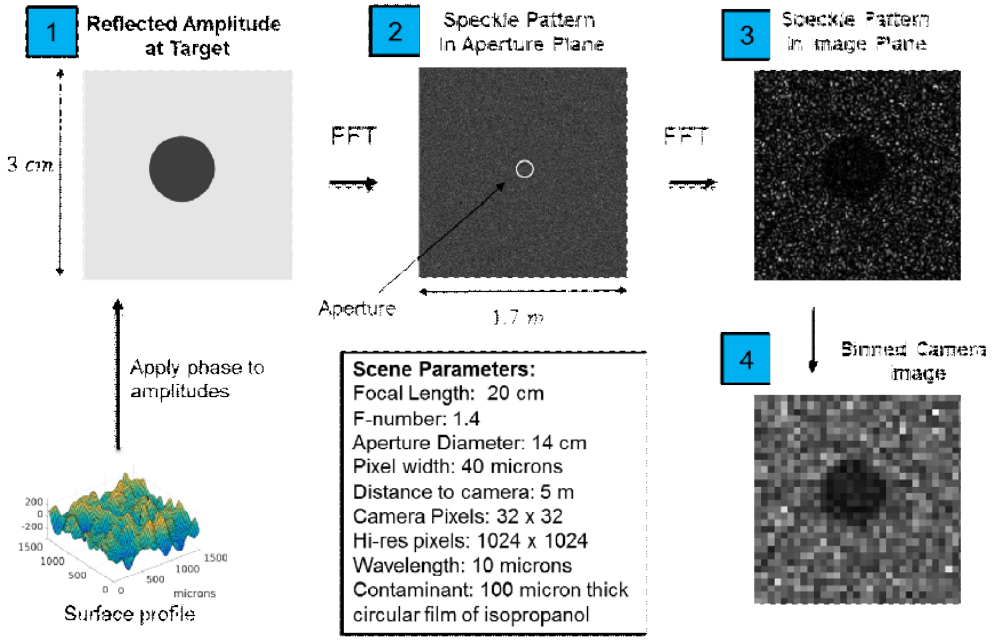


Figure 5: Method for incorporating speckle into synthetic hypercubes.

### 2.7 Example of Synthetic Hypercube and Comparison with Measurements

In this section, we compare a synthetic hypercube generated using the HSI Simulator with experimentally measured results. A measurement was made of a high-density polyethylene (HDPE) substrate, on which chemicals were deposited in the form of our sponsor's logo. Referring to Figure 6a, most of the IARPA logo was drawn using silicone oil while the dot on the letter "i" was formed using triethyl phosphate (TEP). Measurements were made at a standoff distance of 5 meters and at an offset angle of a few degrees to avoid the direct specular reflection. Details regarding the measurement (including a video demonstration) can be found in reference [11]. Figure 6b shows a single frame of a measured hypercube as well as the reflection spectrum due to each chemical. As described previously, for a liquid on a dielectric substrate, a higher reflectance occurs at wavelengths where the chemical is absorbing. The two chemicals can be easily distinguished based on their reflection spectra. Note also the pixel-to-pixel noise which is due to speckle and, to a lesser extent, variations in the thickness of the deposited chemicals. Figure 6c shows a frame of the synthetic hypercube calculated using the HSI Simulator. Each of the chemicals was assumed to have a thickness of 1 μm. Speckle was incorporated assuming a root-mean-square (RMS) surface roughness of 2 μm. The synthetic hypercube visually mimics the measured hypercube with reasonably good fidelity, and the measured spectra are well-matched by simulation.

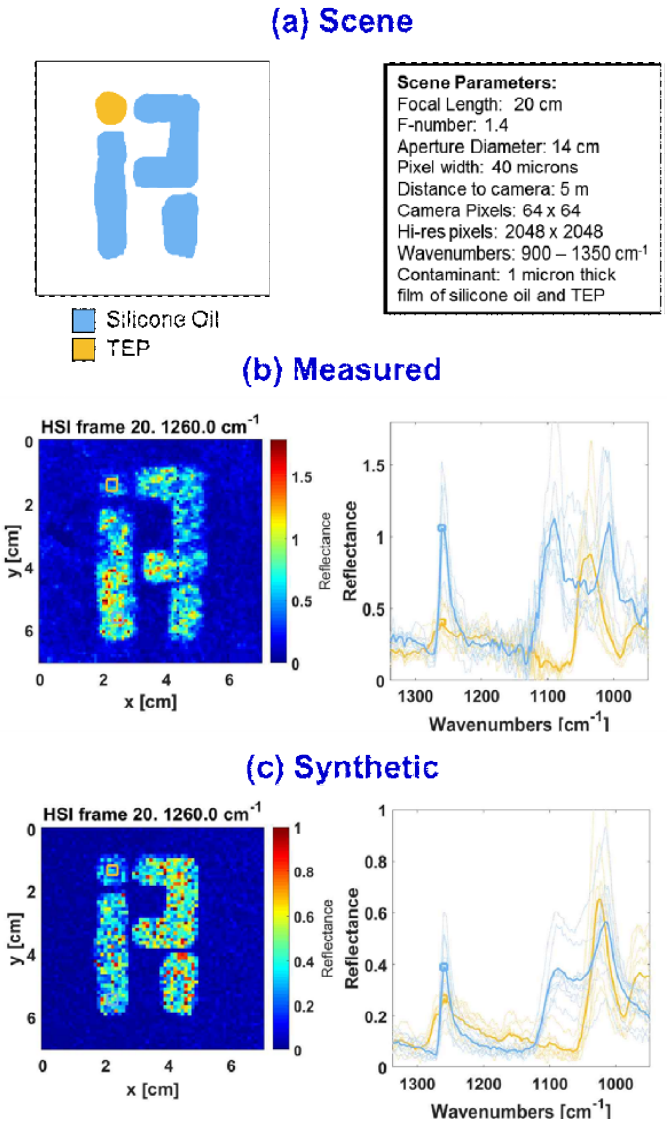


Figure 6: (a) HDPE substrate with the IARPA logo formed from two chemicals, (b) Measured hypercube frame and spectra, and (c) Synthetic hypercube frame and spectra as calculated using the HSI Simulator.

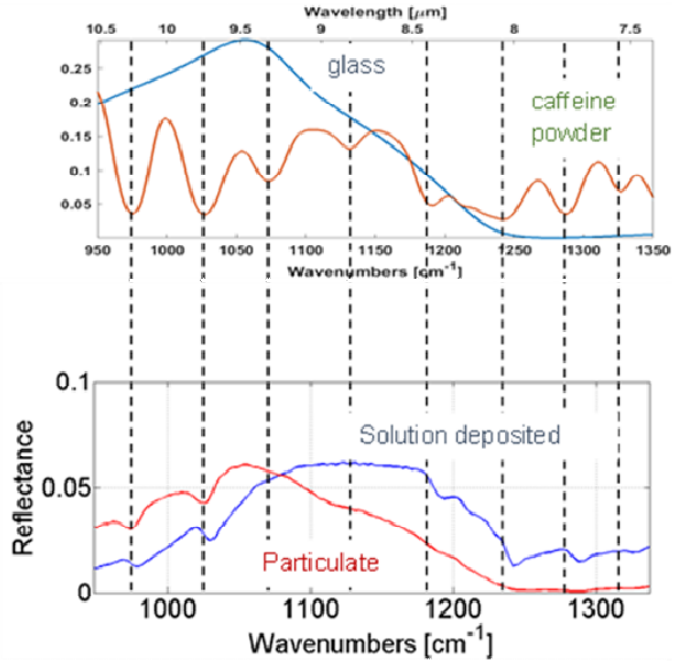


Figure 7: (top) Reflectance of soda-lime glass and the hemispherical diffuse reflectance from caffeine powder. (bottom) Reflectance of trace-levels of caffeine for two separate deposition methods on soda-lime glass.

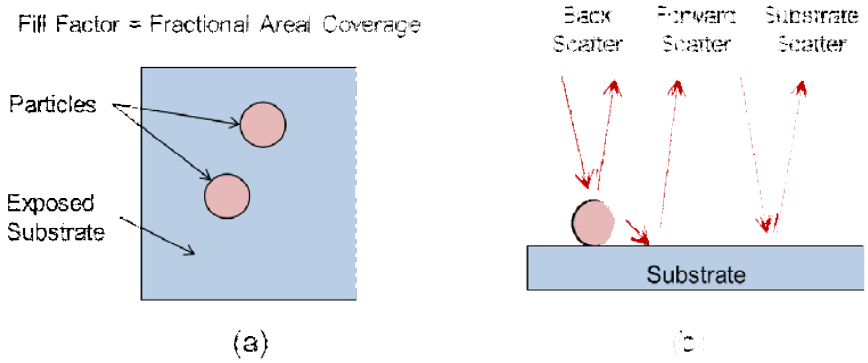


Figure 8: (a) Top-view of substrate with isolated particles, and (b) side-view showing various components of the signature model.

### 2.8 Model for Surfaces Contaminated with Solid Particles

Several signature models are being investigated in order to model solid particles and solid-residues on surfaces as accurately as possible. Here, we describe a particularly simple model that is based on measured diffuse reflectance from powders, $R_{powder}$, and the measured reflectance spectrum for the substrate, $R_{sub}$.

The top portion of Figure 7 plots both the diffuse reflectance of caffeine powder and the specular reflectance of soda-lime glass. Details of these measurements are given in reference [11]. The lower graph in Figure 7 plots the measured reflectance of caffeine on soda-lime glass for two different deposition conditions. The model being described here is

applicable for the case of particles of caffeine (rather than solution-deposited caffeine). One can see that the minima in reflectance occur at the same wavenumbers for the powder and for the particulates on glass. For particulates on glass, however, the overall shape of the curve is strongly modulated by the reflectance of the glass substrate. This naturally leads to the following simple model in which the total reflection spectrum is calculated based on the three different paths the incident light can take as shown in Figure 8

$$\rho_{\Omega,target} = (1 - FF) \cdot \rho_{\Omega,\mathrm{sub}} + FF \cdot \rho_{\Omega,powder} \left( C_{bs} + C_{fs} R_{sub} \right).$$

where $\rho_{\Omega,powder} = R_{powder} / (\pi \text{ sr})$. Here, the first term is simply the direct reflectance from the substrate. The second term contains back reflectance from the particles, as well as the light that scatters off both the particle and the substrate. These factors are scaled using the particle fill factor, *FF*, and two fit parameters $C_{back}$ and $C_{fwd}$. Figure 9 plots the measured reflection spectra for particulates of the explosives RDX and PETN on soda-lime glass. These measurements were made at a range of 0.6 m [11]. The black curve is the measured reflectance, while the blue curve is the fit using the expression given above. The correspondence is surprisingly good given the simplicity of the model. Again, we are continuing to refine the model to bring it into closer agreement with measurements.

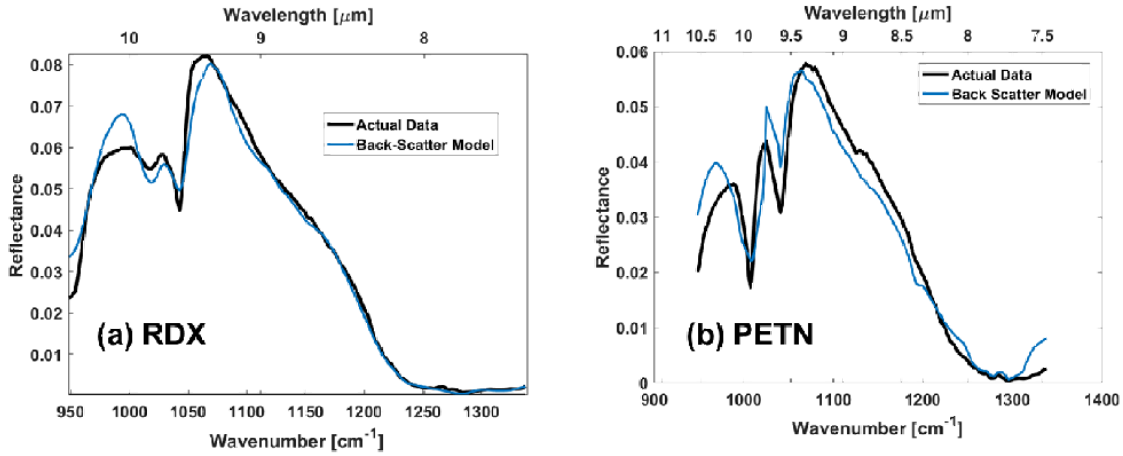


Figure 9: Measured (dark blue) and calculated (light blue) reflectance of (a) RDX and (b) PETN particles on soda-lime glass. The calculation is based on a simple that model that based on measured powder reflectance.

## 3. SUMMARY

We describe a simulator for a laser-based standoff chemical detection system that utilizes MIR HSI. Our goal is to generate synthetic hypercubes that match experimental results with enough fidelity to be useful for the development of detection algorithms that cover a wide application space. The HSI Simulator incorporates signature models for liquids and solids on various surfaces, as well as gases. Also included are effects related to speckle noise and detector noise. Good correspondence has been achieved with signature models for both liquid and solid contaminants. Work is ongoing to further refine and improve upon the accuracy of the signature models.

## 4. AKNOWLEDGEMENTS

We gratefully acknowledge the support of the IARPA SILMARILS program through AFRL contract FA8650-16-C-9107. We also thank the Applied Physics Laboratory at Johns Hopkins University (JHU/APL) and the Naval Research Laboratory (NRL) for providing samples, and to the Pacific Northwest National Laboratory (PNNL) for providing reference spectral data.

## REFERENCES


[1] Goyal, A. K. and Myers, T. R., "Active mid-infrared reflectometry and hyperspectral imaging", chapter in [Laser-Based Optical Detection of Explosives] CRC Press (2015).

[2] Phillips, M. C. and Bernacki, B. E., "Infrared spectroscopy of explosive residues: Measurement techniques and spectral analysis," chapter in [Laser-Based Optical Detection of Explosives] CRC Press (2015).

[3] Goyal, A. K., et al., "Active infrared multispectral imaging of chemicals on surfaces," Proc. SPIE 8018, 80180N (2011).

[4] Goyal, A. K., et al., "Active hyperspectral imaging using a quantum cascade laser (QCL) array and digital-pixel focal plane array (DFPA) camera," Opt. Express 22, 14392 (2014).

[5] Ostendorf, R., et al., "Recent Advances and Applications of External Cavity-QCLs towards Hyperspectral Imaging for Standoff Detection and Real-Time Spectroscopic Sensing of Chemicals," Photonics, 3(2), 28 (2016).

[6] Phillips, M. C., et al.., "Challenges of infrared reflective spectroscopy of solid-phase explosives and chemicals on surfaces," Proc. SPIE 8358, 83580T (2012).

[7] Suter, J. D., Bernacki, B. E., and Phillips, M. C., "Spectral and angular dependence of mid-infrared diffuse scattering from explosives residues for standoff detection using external cavity quantum cascade lasers," Appl. Phys. B 108, 965 (2012).

[8] Raz, G., et al., "Novel Trace Chemical Detection Algorithms: A Comparative Study," Proc SPIE 10198 (2017).

[9] Ghatak, A. K., Thyagarajan, K., and Shenoy, M. R., "Numerical analysis of planar optical waveguides using matrix approach," J. Lightwave Techn. LT-5, 660 (1987).

[10] Goodman, J. W., [Speckle phenomena in optics: Theory and applications], Ben Roberts, Englewood (2007).

[11] Kelley, D. B.., et al., "High-speed mid-infrared hyperspectral imaging using quantum cascade lasers," Proc. SPIE 10183 (2017).